metals

MDPI

Article

Experimental and Numerical Study on the Energy Absorption of Polyurethane Foam-Filled Metal/Composite Hybrid Structures

Shuguang Yao [1,2,3], Zhifang Chen [1,2,3], Ping Xu [1,2,3,4,*], Zhixiang Li [1,2,3] and Ziliang Zhao [1,2,3]

1 Key Laboratory of Traffic Safety on Track, Ministry of Education, School of Traffic & Transportation Engineering, Central South University, Changsha 410075, China; ysgxzx@csu.edu.cn (S.Y.); zhifangchen@csu.edu.cn (Z.C.); ashinelp@csu.edu.cn (Z.L.); 184211040@csu.edu.cn (Z.Z.)
2 Joint International Research Laboratory of Key Technology for Rail Traffic Safety, Central South University, Changsha 410075, China
3 National & Local Joint Engineering Research Center of Safety Technology for Rail Vehicle, Central South University, Changsha 410075, China
4 State Key Laboratory of High Performance Complex Manufacturing, Central South University, Changsha 410075, China
* Correspondence: xuping@csu.edu.cn; Tel.: +86-1527-315-1699

Abstract: Hybrid structures have the advantage of combining different types of materials at the same time. The trend of lightweight design in the transportation industry has promoted the development and application of composite materials with good crashworthiness performance. Low-density crushable foam-filled metal-composite hybrid structures have potential advantages as energy-absorbing components. This study investigated the mechanical characteristics of four different polyurethane foam-filled hybrid structures and their individual components under quasi-static axial compression. The experimental results showed foam-filled hybrid structures could change the deformation mode and improve stability during the compression process. Meanwhile, these hybrid structures could also improve energy absorption compared with their individual components. Among the different configurations, specimen C-PU-C (i.e., polyurethane foam filler between an outer CFRP tube and an inner CFRP tube) had the highest energy absorption capacity, at 5.4 kJ, and specific energy absorption, at 37.3 kJ/kg. Finally, a finite element (FE) model was established to analyze the mechanical characteristics of the hybrid structures by validating the simulation results against the experimental results.

Keywords: hybrid structure; aluminum alloy; composite material; polyurethane foam; energy absorption

Citation: Yao, S.; Chen, Z.; Xu, P.; Li, Z.; Zhao, Z. Experimental and Numerical Study on the Energy Absorption of Polyurethane Foam-Filled Metal/Composite Hybrid Structures. *Metals* **2021**, *11*, 118. https://doi.org/10.3390/met11010118

Received: 21 November 2020
Accepted: 7 January 2021
Published: 9 January 2021

1. Introduction

Thin-walled structures have been widely used as energy-absorbing components in transportation and aerospace engineering; meanwhile, the strong demand for high performance and light weight is encouraging the application of different structural configurations and materials. Sandwich structures, which comprise two thin hard face sheets and an inner core, are an effective type. In general, face sheets are made of a metal- or fiber-reinforced composite, and the core is made of honeycomb, metallic or polymer foam. Typical sandwich structures under compression conditions include sandwich tubes [1], beams [2,3] and panels [4,5]; they have good energy absorption behavior and high specific energy absorption under quasi-static or impact loading conditions. Sandwich tubes can enhance their light weight and crashworthiness by using different materials to guide deformation modes and to absorb as much energy as possible.

The mechanical behavior of thin-walled metal tubes under quasi-static and impact loading conditions has been extensively investigated in the past decades. For example,

Andrews et al. [6] classified the failure modes as concertina, diamond, mixed and Euler buckling modes. Subsequently, more researchers focused on the application of aluminum alloy for the advantage of light weight. In addition, some thin-walled tubes with special shapes are able to improve crashworthiness performance. For example, Yao et al. [7] investigated the crashworthiness of circular hybrid corrugated tubes under axial compression, and they had better energy absorption capacity than ordinary corrugated tubes. Li et al. [8] investigated the crashworthiness of corrugation-reinforced multi-cell square tubes, which also exhibited high energy absorption capacity and good weight efficiency. Meanwhile, the mechanical behavior of thin-walled metal tubes can be predicted by the given geometry and material parameters, and validation using the finite element method (FEM) has been demonstrated [9–11].

In addition, composite materials have attracted increasing attention for their great potential with respect to their light weight, and carbon fiber-reinforced plastic (CFRP), as one a typical class of composite materials, is gradually being used in transportation. Compared with traditional metallic materials, composites exhibit higher stiffness, higher strength and lower density, so they have good potential with regard to crashworthiness and light weight [12,13]; however, their cost is higher than metal now. In contrast to metal tubes, the primary energy absorption mechanisms of thin-walled CFRP tubes are fracture failure modes such as delamination between laminates, fiber breakage, and matrix cracking [14]. The energy absorption capability and specific energy absorption of thin-walled CFRP tubes are better than those of aluminum tubes with a similar shape [15]. Therefore, researchers have focused on the crashworthiness of metal–composite hybrid tubes, combining the advantages of the two materials. Zhu et al. [16] compared the mechanical behaviors of metal/CFRP hybrid structures under static and dynamic loading, and unlike Al tubes, the energy-absorbing capacity of the CFRP tubes decreases considerably under dynamic loading condition. Wang et al. [17] investigated how to achieve the best possible balance between the performance and the cost of hybrid structures by means of multi-objective optimization. Hussein et al. [18] studied an energy dissipating mechanism for crushing square Al/CFRP tubes; specially designed platens were used to reduce the initial peak crushing force and increase the energy absorption of the CFRP tubes. Some researchers have focused on multi-cell hybrid tubes and structural multi-objective optimization [19,20]. In addition, the finite element method (FEM) is able to simulate composite structures under quasi-static and dynamic loading. For example, Batuwitage et al. [21] investigated the impact behavior of CFRP strengthened square hollow steel tubes by numerical simulation.

For foam-filled sandwich structures, aluminum honeycomb, aluminum foam and polyurethane (PU) foam can be used as good fillers to absorb energy. On the other hand, composite tube-reinforced foams or honeycomb also exhibit remarkable crashworthiness performance [22–24]. Li et al. [25] compared the crashworthiness of empty and Al foam-filled thin-walled tubes, and foam-filled circular tube structures possessed high energy-absorbing efficiency. Sun et al. [26] compared the crashworthiness of empty circular CFRP with CFRP/aluminum/steel tubes filled with Al foam or honeycomb under axial quasi-static compression, this study showed the potential of foam/honeycomb-filled CFRP tubes as energy absorbers. Zhu et al. [27] investigated the crashworthiness behavior of a circular Al tube internally reinforced with a composite skeleton and Al foam under quasi-static loading, with the tests showing that the strong interaction between foams and the skeleton had a very noticeable contribution towards total energy absorption. Zheng et al. [28] investigated the influence of some parameters on the mechanical behavior of Al foam-filled Al/CFRP hybrid tubes under quasi-static axial compression. PU foam is the most commonly used polymeric foam [29], and it is used as the filler in energy absorption systems in a variety of applications such as bumpers for bridge protection [30,31], blast-resistant connectors [32,33], and various kinds of folded structures [34,35]. Hussein et al. [36] compared the compressive response of square Al tubes filled with PU foam and Al honeycomb, and the tubes that were filled with both PU foam and Al honeycomb exhibited obvious performance improvement. Gan et al. [37] investigated the mechanical behaviors of foam-filled

CFRP and Al thin-walled structures under quasi-static compression, and the experimental results showed that circular CFRP tubes filled with PU foam had better energy absorption capacity than square and hexagonal structures. In addition, the SEA of the CFRP tube filled with PU foam was higher than that of the Al tube filled with Al foam.

As mentioned above, Al foam-filled sandwich structures have been investigated widely, but there research is lacking on PU foam as filler. This work aims to study the crashworthiness characteristics of PU foam-filled Al/CFRP tubes with different hybrid configurations. Firstly, a series of quasi-static axial compression tests for empty and foam-filled Al/CFRP hybrid tubes was carried out to explore their mechanical behavior. Secondly, the deformation mode and energy absorption demonstrated in these experimental results were investigated. Then, some economic indicators were considered to evaluate their energy absorption performance. Finally, numerical models were built in Abaqus/Explicit and validated by experimental results

2. Experiments

2.1. Preparation of Specimens

In this study, the CFRP tubes were made in prepregs with T300 0/90° woven carbon fabric and epoxy. In addition, the aluminum tubes were made of AA6061. There are two kinds of tubes for CFRP and Al: outer and inner tubes, respectively. The length and the thickness of all tubes were 150 mm and 1.5 mm, respectively, and there were six plies, with a stacking sequence of $(0°, 90°)_3$. In addition, the outer tubes, which had a diameter of 60 mm, were designated as CFRP-O and AL-O, respectively. In addition, the inner tubes, which had a diameter of 35 mm, were designated as CFRP-I and AL-I, respectively. The density of the PU foam was 0.2 g/cm^3. The length and the diameter of the PU foam column used to test the material characterization were 100 mm and 56 mm, respectively. The diameter and the thickness of hollow PU foam columns, the length of which was the same as the tubes, were 56 mm and 10 mm, respectively. The manufacturer of all the specimens was YHXK Co., Ltd. in China. Table 1 summarizes the geometric dimensions of all the specimens for the experimental study. In addition, four foam-filled hybrid structures were prepared as shown in Figure 1a, C-PU-AL denotes the hybrid configuration with a CFRP outer tube, a foam core and an Al inner tube; the rest can be determined in the same manner.

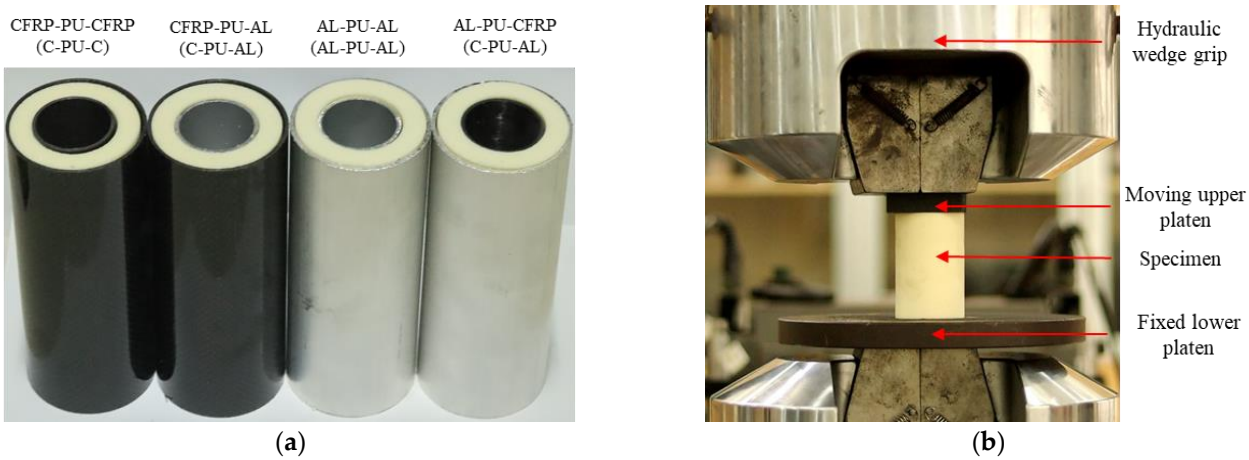

(**a**) (**b**)

Figure 1. Preparation of specimens and quasi-static compression tests. (**a**) Four foam-filled hybrid structures; (**b**) quasi-static compression test configuration.

Table 1. Summary of all the specimen for the experimental study.

Specimens	Thickness (mm)	Weight (g)	Diameter D (mm)	Length (mm)	Density ρ (g/cm^3)	Materials
CFRP-I	1.5	36.9	35	150	1.5	T300/epoxy
CFRP-O	1.5	64.5	60	150	1.5	T300/epoxy
AL-I	1.5	63.9	35	150	2.7	AA6061
AL-O	1.5	111.6	60	150	2.7	AA6061
Foam	-	49.2	56	100	0.2	Polyurethane
Foam-H	10	43.3	56	150	0.2	Polyurethane
AL-PU-AL	-	218.8	60	150	-	AL-PU-AL
AL-PU-C	-	191.8	60	150	-	AL-PU-CFRP
C-PU-AL	-	171.7	60	150	-	CFRP-PU-AL
C-PU-C	-	144.7	60	150	-	CFRP-PU-CFRP

2.2. Material Characterization

To develop effective numerical models, tests were conducted on CFRP, Al and PU foam materials to obtain the mechanical properties in accordance with the ASTM D3039 and D3518 procedures in an MTS Landmark testing machine at room temperature, as shown in Figures 1b and 2. The stress–strain curves of AL, PU foam and CFRP materials are shown in Figure 3.

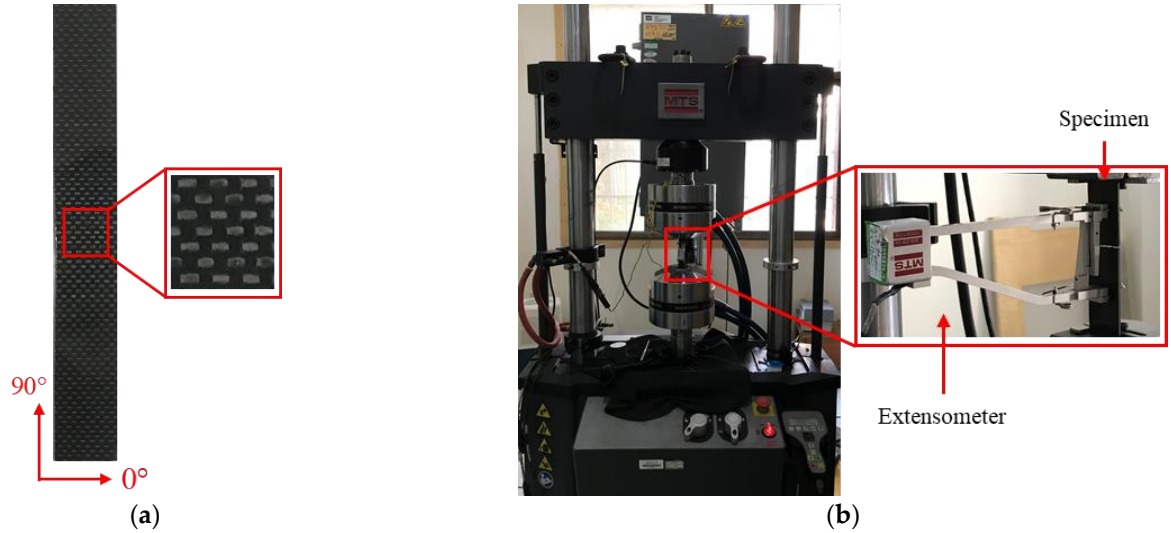

Figure 2. Specimens for tensile test. (**a**) Specimen and fiber orientation for the tensile test; (**b**) tensile test configuration.

2.3. Quasi-Static Compression Tests

All the quasi-static compression tests were implemented in a standard MTS 322 universal testing machine with a loading capacity of 500 kN at room temperature, as shown in Figure 1b. All tests were carried out at a constant speed of 2 mm/min. The final crushing distance was 80 mm, which was more than half of the original length of the specimen. The force and displacement data were completely recorded by the system and the deformation of specimens were photographed in detail.

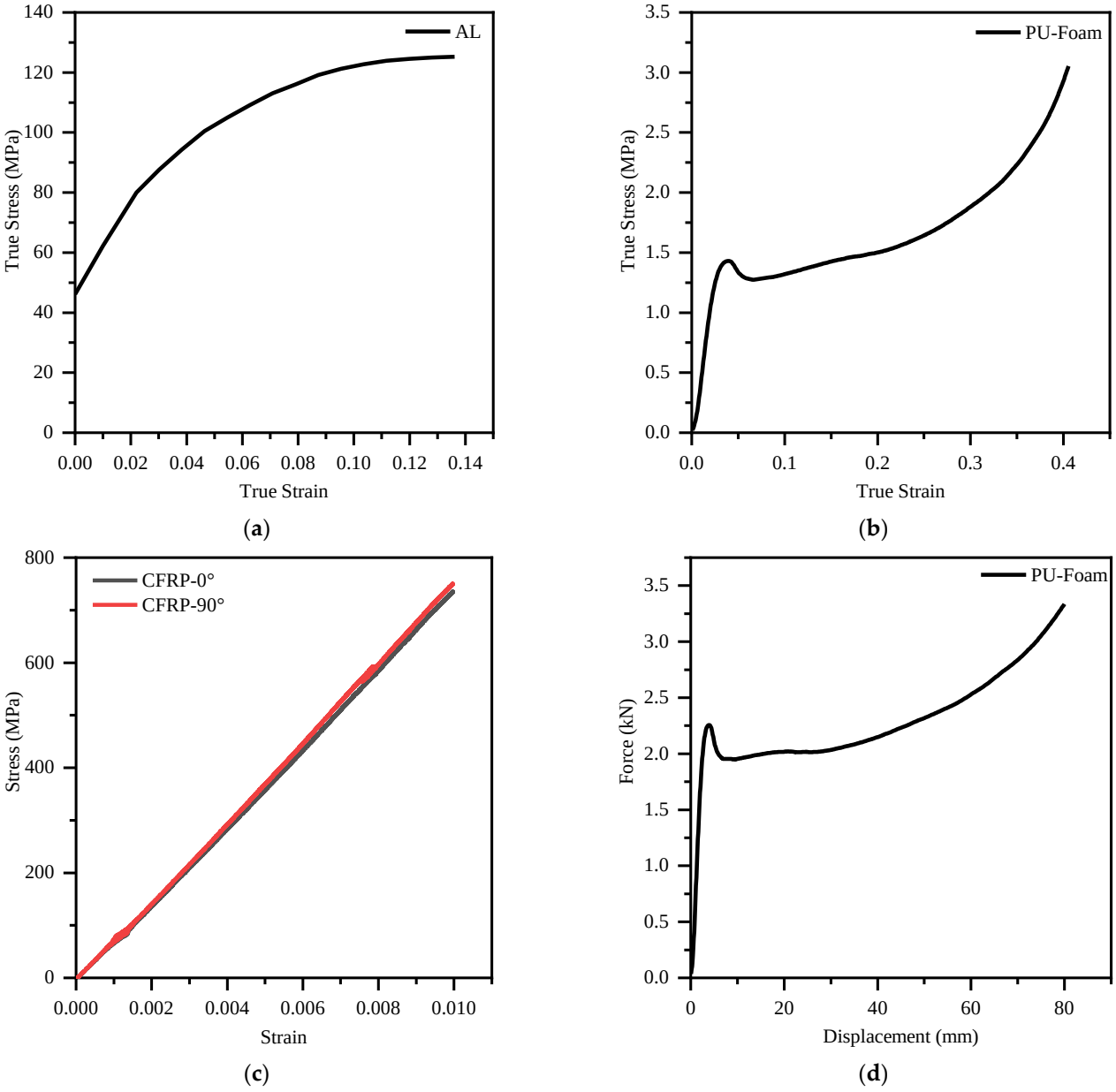

Figure 3. Experimental results of the material tests. (**a**) Stress–strain curve of AL; (**b**) stress–strain curve of PU foam; (**c**) stress–strain curve of CFRP; (**d**) force–displacement curve of PU foam under quasi-static compression.

2.4. Crashworthiness Indicators

In this study, several widely used indicators were used to evaluate the crashworthiness of these single tubes and hybrid structures, including energy absorption (*EA*), specific energy absorption (*SEA*), mean crushing force (*MF*) and peak crushing force (*PCF*).

Energy absorption (*EA*) measures the total strain energy absorbed by the structure during the crushing process, which is determined in terms of the area under the force–displacement curve, defined as:

$$EA = \int_0^d F(x)dx \tag{1}$$

where d is crushing displacement.

The specific energy absorption (*SEA*) means energy absorption in unit mass, defined as:

$$SEA = \frac{EA}{m} \tag{2}$$

so materials with a higher SEA may be helpful for the lightweight design of structures.

The mean crushing force (*MF*) is used to show the average level of force, for a given crushing distance d, defined as:

$$MF = \frac{EA}{d} \tag{3}$$

In addition, the peak crushing force (*PCF)* is the maximum value of force during the compression process. Generally, *PCF* appears in the initial stage of the compression process. In addition, a higher *PCF* possibly means a relatively higher vehicle deceleration, which increases the risk of occupants being injured in a collision accident. Thus, lower *PCF* values are preferred.

3. Numerical Models

3.1. Finite Element Modeling

The finite element (FE) model was built in the commercial finite element method software ABAQUS/Explicit. Figure 4 illustrates the finite element (FE) model of the specimen C-PU-AL, which consists of five parts. Both the upper and the lower plate were modeled using discrete rigid elements, the upper plate moves and the lower plate is fixed. The CFRP tube was modeled in six layers and meshed with continuum shell elements (SC8R) with a size of 1.0 mm × 1.0 mm × 0.25 mm. Cohesive elements with the same size as CFRP were adopted here to capture the delamination behaviors between the adjacent laminates. The aluminum tube was meshed using S4R elements with a size of 1.0 mm × 1.0 mm. In addition, the polyurethane foams were modeled using C3D8R elements with a size of 1.0 mm × 1.0 mm × 1.0 mm. In addition, a general contact with a friction coefficient of 0.2 was used to capture the interaction between these individual components.

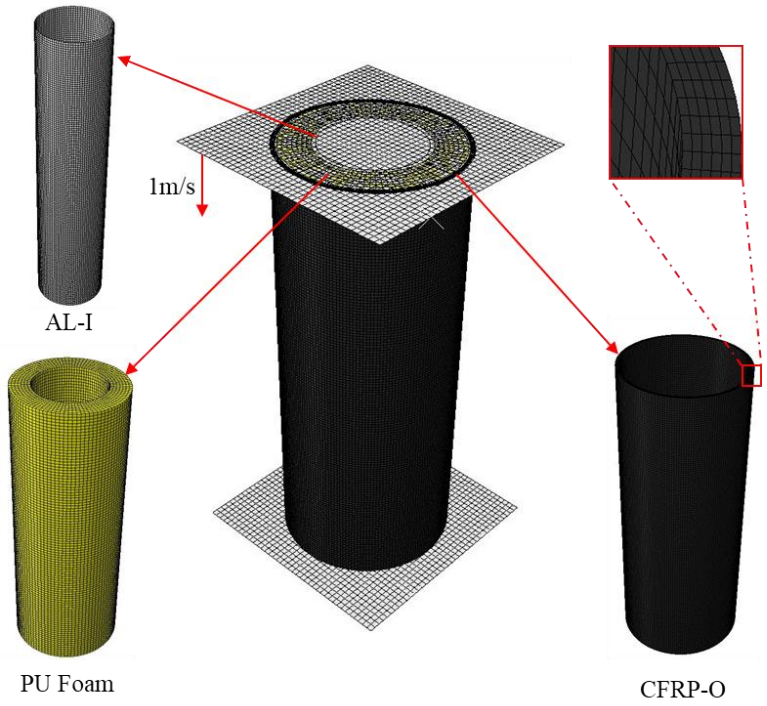

Figure 4. The FE model of the hybrid specimen C-PU-AL (polyurethane foam filler between outer CFRP tube and inner aluminum tube) and individual components.

To improve the calculation efficiency, a much higher loading rate was allowed to simulate the quasi-static experiments in the explicit finite element (FE) analysis, satisfying the requirement that kinetic energy not exceed 5% of internal energy, and that the velocity of the upper crosshead remains constant at 1.0 m/s.

3.2. Material Models

3.2.1. Aluminum Tube

In this study, the aluminum tube was modelled using an elastic-plastic material model based on the von Mises isotropic plasticity algorithm with the following mechanical properties: Young's modulus 70.0 GPa, density 2.7 g/cm^3, and Poisson's ratio 0.3, while the true stress–true strain curve was obtained from the uniaxial test, as plotted in Figure 3a.

3.2.2. Polyurethane Foam

The polyurethane foam was modelled using the *CRUSHABLE FOAM material model with isotropic hardening with following mechanical properties: Young's modulus 49.4 MPa and density 0.2 g/cm^3; the true stress–true strain curve is plotted in Figure 3b.

3.2.3. CFRP Tube

As distinct from the metal tube, the CFRP tube is a kind of multi-layered composite structure. In order to simulate the real physics of the crushing of composites, in this study, the material model of CFRP tube included two parts: one was an intra-laminar constitutive model reflecting the constitutive behaviors of fiber and matrix, and the other was an inter-laminar constitute reflecting the mechanical behaviors of the adhesive layers.

In the intra-laminar constitutive model, composite ply is thought to be a homogeneous orthotropic material, the material parameters describe both the elastic stress–strain relations and the failure behaviors along the fiber directions, as well as matrix cracking under shear loads. The material parameters of the elastic and failure behaviors along the fiber directions used in this study are shown in Table 2.

Table 2. Material parameters of the elastic and failure behaviors along the fiber directions.

Description	Variable	Value
Density(kg/m^3)	ρ	1560
Elastic properties (GPa)	E_1	7.5
-	E_2	7.4
-	G_{12}	5.0
-	ν_{12}	0.04
Damage initiation (MPa)	X_{1+}	789
-	X_{1-}	704
-	X_{2+}	748
-	X_{2+}	698
-	S	107
Fracture energies (kJ/m^2)	G_{fc}^{1+}	95
-	G_{fc}^{1-}	145
-	G_{fc}^{2+}	90
-	G_{fc}^{2-}	140

In the inter-laminar constitutive model, the material parameters describe the adhesive bonds between adjacent plies and simulate the delamination phenomenon. A traction-separation law comprised of a damage criterion based on a quadratic nominal stress criterion and damage evolution based on the Benzeggagh-Kenane fracture criterion. The material properties describing the inter-laminar damage model were the same as those reported in [31].

4. Results and Discussion

4.1. Experimental Results

4.1.1. Aluminum Tubes

Figure 5a,b show the deformation modes and load–displacement curves of the inner aluminum tube (AL-I) and the outer aluminum tube (AL-O), respectively. For AL-I, there were typical concertina modes during the first two deformation process, so it exhibited good stability, and the force was regular and repeatable with crushing displacement changes. However, the deformation mode changed to diamond mode when the crushing displacement reached about 33 mm, the tube wall did not fold completely inward; sharp corners were formed on the opposite side and appeared alternately, so the stability of the deformation process became bad and the force obviously decreased. Finally, the AL-I formed a mixed deformation mode.

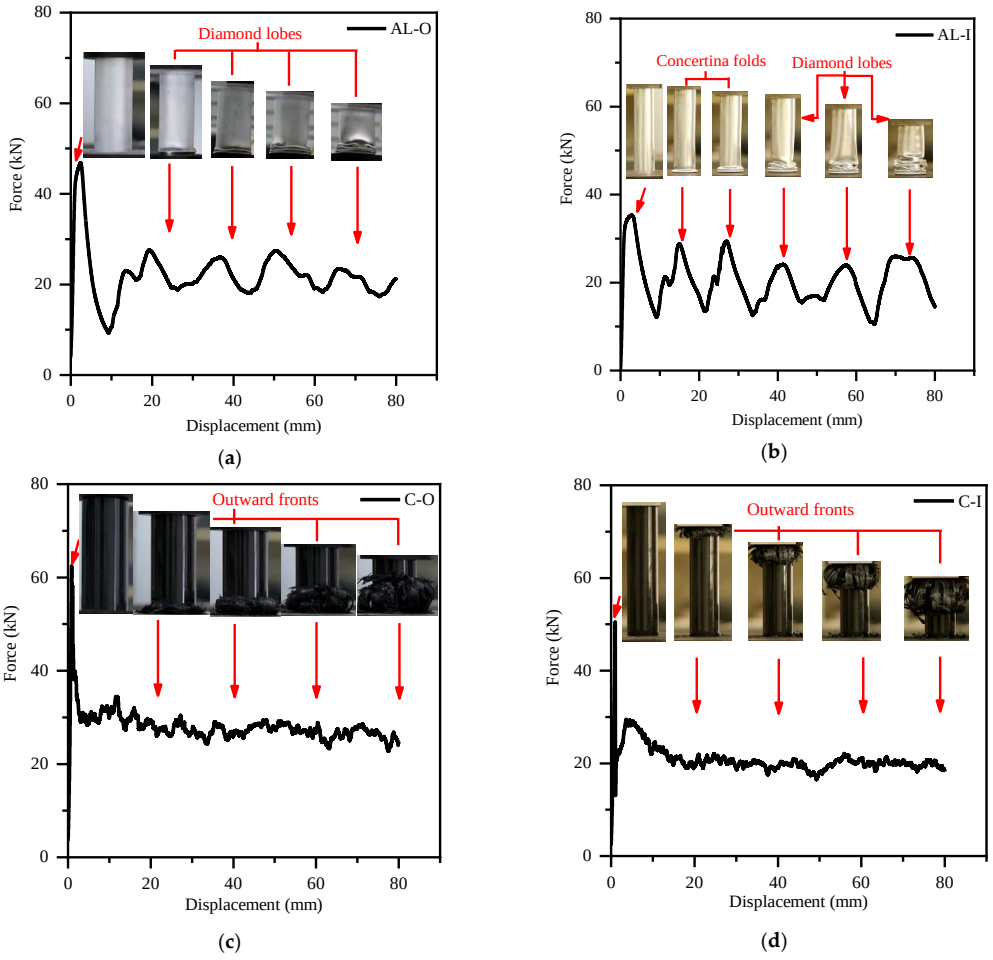

Figure 5. Deformation mode and force–displacement curves of single tubes: (**a**) AL-O; (**b**) AL-I; (**c**) C-O; (**d**) C-I.

For Al-O, the diameter of the tube increased from 35 mm to 60 mm compared with al-I; it exhibited a concertina mode only at the beginning of compression, and then it turned into diamond mode; however, the stability of the compression process seemed worse, the force was irregular and unrepeatable, and it changed within a small range. Compared with the aluminum tube with typical concertina modes throughout the whole compression process, these experimental results showed that deformation mode obviously influences the mechanical behavior, and the energy absorption performance could not be reflected perfectly. However, when the compression process is not under ideal conditions, it would be very helpful to improve the energy absorption performance by having better deformation mode.

4.1.2. CFRP Tubes

Figure 5c,d show the deformation modes and load-displacement curves of the inner CFRP tube (CFRP-I) and the outer CFRP tube (CFRP-O), respectively. Different from the plastic deformation of the aluminum tubes above, the CFRP tubes exhibited obvious breakage and failure during the compression process. At the beginning of compression, similar to the metallic tubes, the CFRP tubes went through an elastic stage, and the force increased rapidly to peak force, following which the force exceeded the load ability of the tube and structure breakage appeared. An initial splaying mode appeared inside and outside due to fiber breakage and delamination, and the force decreased rapidly. Then, the fiber broke mainly along some paths and the compression and force were stable with small fluctuations, and these results show that the force increases with increasing tube diameter; therefore, the CFRP tubes exhibited good energy absorption ability.

4.1.3. PU Foam-Filled AL-AL Hybrid Structure

Figure 6a shows the deformation modes and force–displacement curves of AL-PU-AL. These results show that this hybrid structure helped the outer aluminum tube achieve typical concertina folds throughout the whole compression, with each fold being formed about every 15 mm of compression displacement. The stability of this process was obviously better than that of the single outer aluminum tube above. Then, the structure was cut along the cross-section after the experiment, as shown in Figure 7a. The deformation of the inner aluminum tube was similar to that of the inner aluminum tube (AL-I) above, and the foam core was compressed between two tubes. Therefore, this hybrid structure exhibited a more stable deformation mode.

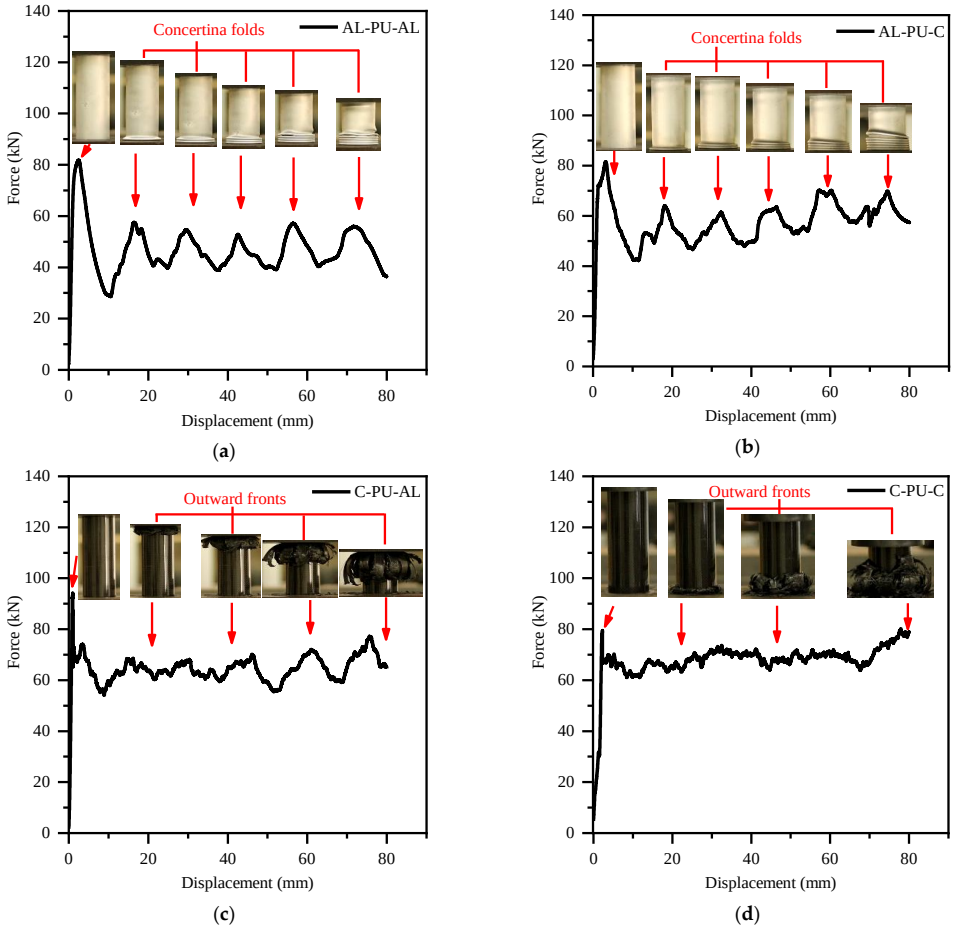

Figure 6. Deformation mode and force–displacement curves of hybrid structures: (**a**) AL-PU-AL; (**b**) AL-PU-C; (**c**) C-PU-AL; (**d**) C-PU-C.

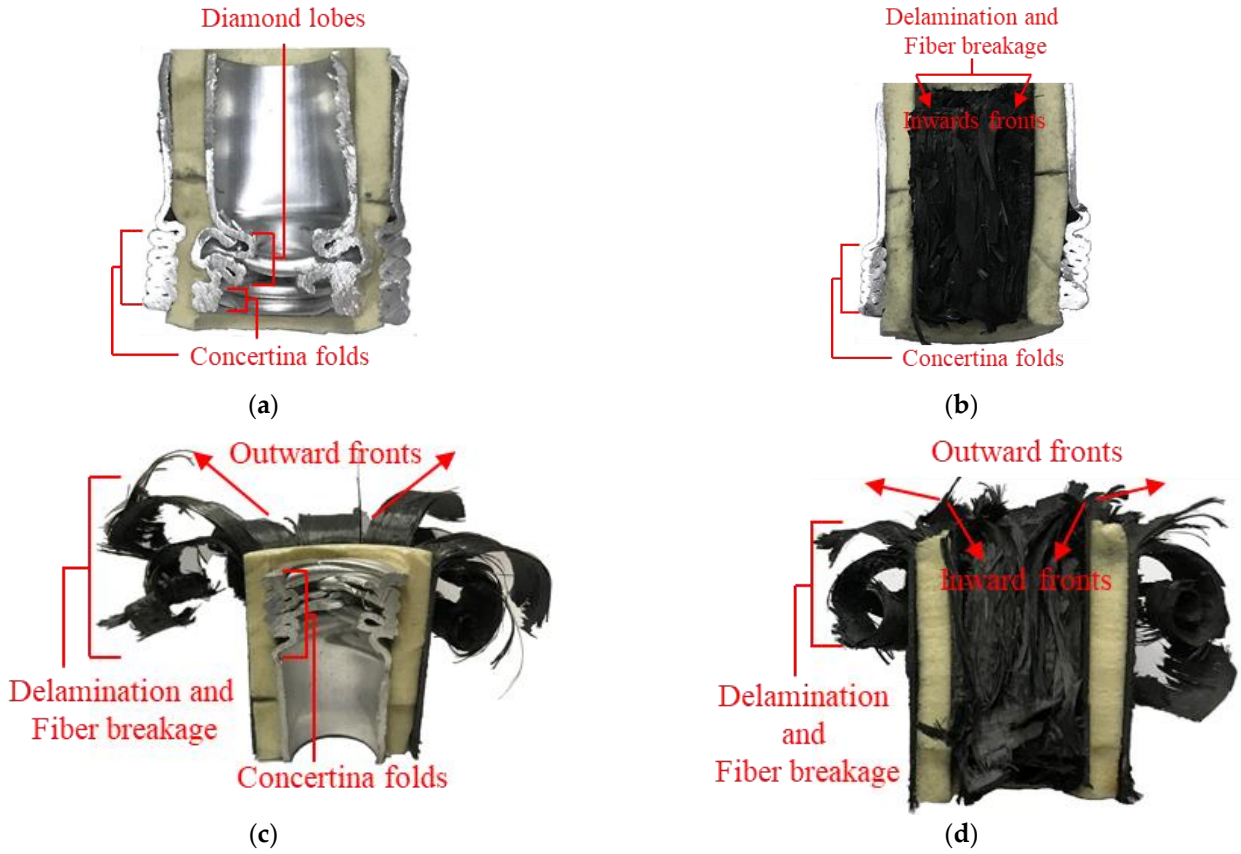

Figure 7. Internal deformation mode of hybrid structures: (**a**) AL-PU-AL; (**b**) AL-PU-C; (**c**) C-PU-AL; (**d**) C-PU-C.

The force of this hybrid structure increased rapidly at the beginning of compression, and when it exceeded the load ability of the structure, the force decreased to a very low value and then changed with deformation. Compared with single aluminum tubes, the force exhibited better repeatability, and this hybrid structure showed better energy absorption ability.

4.1.4. PU Foam-Filled AL-C Hybrid Structure

Figure 6b shows the deformation modes and force–displacement curves of AL-PU-C. Similar to AL-PU-AL, above, this hybrid structure also helped the outer aluminum tube to achieve the typical concertina mode and exhibited good stability during the entire compression. Then, this structure was cut along the cross section after the experiment to investigate the deformation of the inner CFRP tube and the foam core, as shown in Figure 7c. The failure mode of the inner CFRP tube was mainly fiber breakage and delamination, but was obviously different from the single CFRP tube (C-I). All of the fiber was gathered inside and it was largely restricted by the foam core. For the foam core, the side closer to the outer aluminum tube was compressed by its plastic deformation, and the other side was not obviously influenced by the CFRP tube. Therefore, this hybrid structure also exhibited a more stable deformation mode.

The force–displacement curve of this hybrid structure mainly exhibited the mechanical properties of the outer aluminum tube, but at the final stage of compression, the force increased. Part of the reason for this was that the foam core was compressed to densification. Compared with the single aluminum tubes, this hybrid structure showed better energy absorption ability.

4.1.5. PU Foam-Filled C-AL Hybrid Structure

Figure 6c shows the deformation modes and force–displacement curves of C-PU-AL. The outer CFRP tube exhibited a typical deformation mode similar to the single outer CFRP tube, and this hybrid structure showed good stability during compression. Then, the hybrid structure was cut along the cross section after the experiment, as shown in Figure 7c. Different from the single outer CFRP tube, all fiber damage developed outwards, and was restricted by the foam core.

The force–displacement curve of this hybrid structure fluctuated less than the individual structures above and exhibited the mechanical properties of the outer CFRP tube. In addition, the peak force was higher. At the final stage of compression, the force also increased. Compared with single CFRP tubes, this hybrid structure showed better energy absorption ability.

4.1.6. PU Foam-Filled C-C Hybrid Structure

Figure 6d shows the deformation modes and force–displacement curves of C-PU-C. The final deformation mode showed that the outer and inner CFRP tubes were outward fronts and inward fronts, respectively, as shown in Figure 7d. The force–displacement curve of this hybrid structure exhibits the typical mechanical properties of CFRP tubes; it fluctuated a little, and the peak force was close to the mean force, so the area enclosed by the curve and the coordinate axis were bigger and showed better energy absorption ability.

4.2. Comparsion of Hybrid Structures and Their Individual Components

Table 3 shows a summary of the crashworthiness indicators of the single tubes and hybrid structures obtained from the experimental results. For single tubes, the peak forces of AL-O, C-O, AL-I, C-I were 46.8 kN, 62.4 kN, 35.2 kN, and 50.5 kN, respectively. The peak forces of CFRP tubes of the same size were 33.3%, 43.5% higher than aluminum tubes, respectively. The energy absorption of AL-O, C-O, AL-I, C-I were 1.8 kJ, 2.3 kJ, 1.6 kJ, and 1.7 kJ, respectively. Therefore, C-O absorbed 26.7% more energy than AL-O, and C-I absorbed nearly the same amount of energy as AL-I. The mean forces of AL-O, C-O, AL-I, C-I were 22 kN, 27.8 kN, 20.5 kN, and 20.7 kN, respectively. For CFRP tubes, their forces were close to the mean forces. The specific energy absorption of AL-O, C-O, AL-I, C-I was 15.8 kJ/kg, 34.6 kJ/kg, 44.9 kJ/kg, and 25.6 kJ/kg, respectively. Therefore, the CFRP tubes exhibited an obvious advantage in terms of lightweight design as energy absorption components.

Table 3. Summary of crashworthiness indicators of single tubes and hybrid structures obtained from the experimental results.

Specimens	EA (kJ)	SEA (kJ/kg)	PF (kN)	MF (kN)
CFRP-I	1.7	44.9	50.5	21.3
CFRP-O	2.3	34.6	62.4	28.8
AL-I	1.6	25.6	35.2	20.0
AL-O	1.8	15.8	46.8	22.5
Foam-H	0.2	4.6	-	2.5
AL-PU-AL	3.7	16.9	81.8	46.3
AL-PU-C	4.6	24.0	81.5	57.5
C-PU-AL	5.2	30.3	94.1	65.0
C-PU-C	5.4	37.3	79.5	67.5

For hybrid structures, the peak forces of AL-PU-AL, AL-PU-C, C-PU-AL, C-PU-C were 81.8 kN, 81.5 kN, 94.1 kN, and 79.5 kN, respectively. The energy absorption of AL-PU-AL, AL-PU-C, C-PU-AL, C-PU-C was 3.7 kJ, 4.6 kJ, 5.2 kJ, and 5.4 kJ, respectively. Therefore, the C-PU-C hybrid structure exhibited the highest energy absorption capacity The specific energy absorption of AL-PU-AL, AL-PU-C, C-PU-AL, C-PU-C was 16.9 kJ/kg, 24.0 kJ/kg,

30.3 kJ/kg, and 37.3 kJ/kg, respectively. Therefore, the C-PU-C hybrid structure exhibited an obvious advantage in terms of lightweight design as energy absorption components.

Figure 8 shows the force–displacement curves and energy absorption–displacement curves of hybrid structures and the sum of their individual components (SIC). For AL-PU-AL, at the initial stage, the peak force of the hybrid structure was almost equal to the sum force of its individual components, and then the force of the hybrid structure was higher. During the plastic deformation process, the peak force of SIC was about 50 kN, and the peak force of hybrid structure was at first about 55 kN, then it increased gradually when the compression displacement reached about 55 mm, mainly because of the ideal deformation mode and the compression of PU foam, and it increased to about 55.9 kN at 71.8 mm. The energy absorption of this hybrid structure was 3.7 kJ, just 0.1 kJ higher than the energy absorption of SIC. Therefore, this hybrid structure assisted with exhibiting a more stable deformation mode, but did not possess any obvious advantages in terms of improved energy absorption.

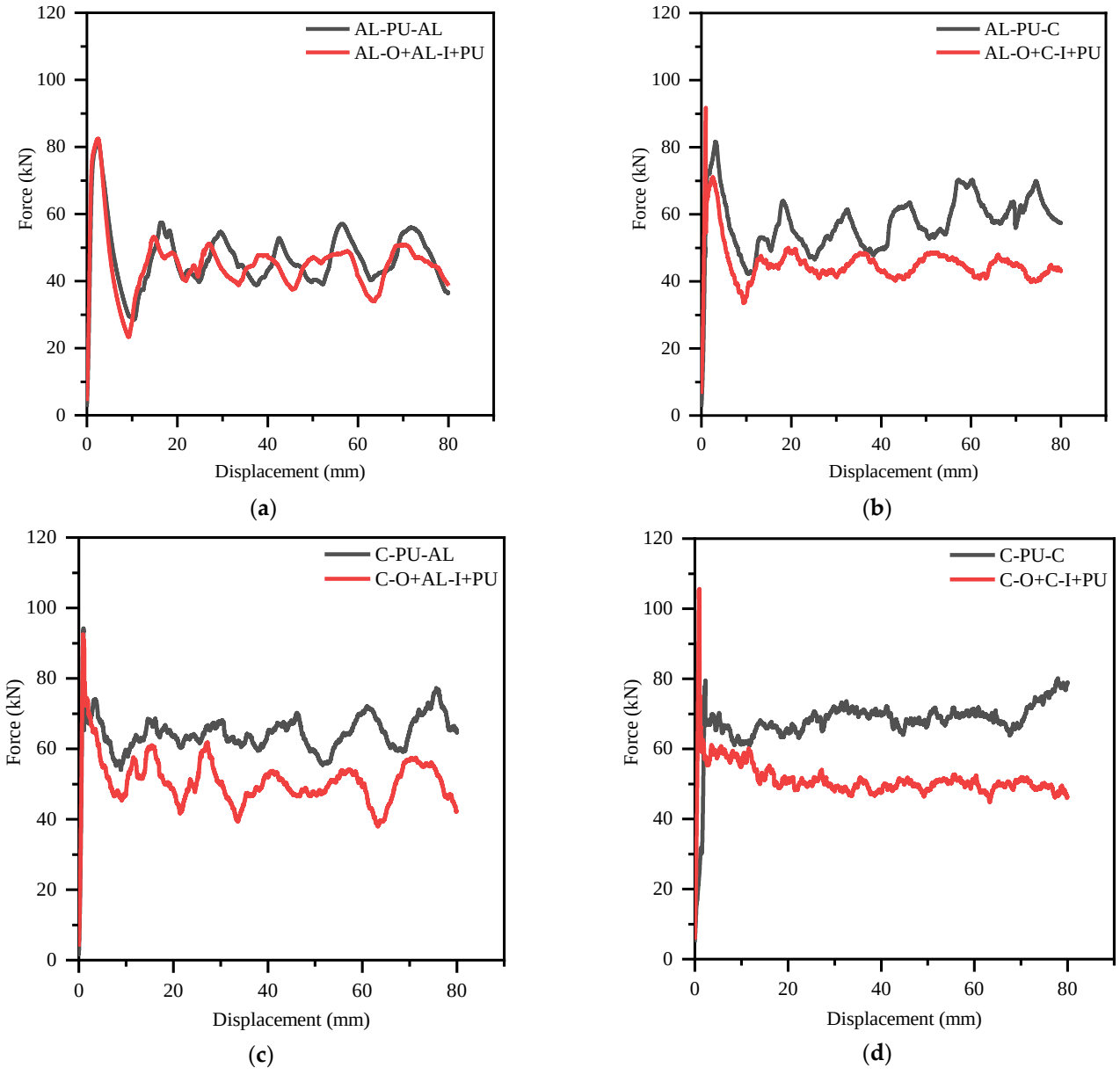

Figure 8. Comparison of force–displacement curves of hybrid structures and sum of their individual components: (**a**) AL-PU-AL; (**b**) AL-PU-C; (**c**) C-PU-AL; (**d**) C-PU-C.

For AL-PU-C, at the initial stage, the peak force of the hybrid structure was not equal to the sum force of its individual components. It was found that AL-O and C-I did not reach peak force at the same time. Here, the two peak forces of C-I and AL-O of SIC were 91.7 kN and 71.2 kN, respectively, and the peak force of this hybrid structure was between them. During the compression process, the force of the hybrid structure was always much higher than SIC, the peak force of SIC was about 50 kN, and the peak force of the hybrid structure was about 63 kN at first, then increased gradually when compression displacement reached about 56.2 mm, and then increased to 69.9 kN at 74.4 mm finally. The energy absorption of the hybrid structure was 4.6 kJ, and 1.0 kJ higher than the energy absorption of SIC. Therefore, this hybrid structure also exhibited a stable deformation mode. Compared with AL-PU-AL, above, the force and energy absorption of the hybrid structure were much higher.

For C-PU-AL, at the initial stage, the peak force of the hybrid structure was almost equal to the sum force of its individual components. During the compression process, the force of the hybrid structure was always much higher than SIC; the force of SIC changed periodically and reflected the characteristic of metal tubes, but the force of the hybrid structure changed slightly in the first half of the stroke and reflected the characteristics of the outer CFRP tube, then it changed periodically gradually. The peak force of SIC was about 61.5 kN, and the peak force of the hybrid structure was about 68.1 kN at first, then it increased gradually when compression displacement reached about 68.5 mm, and finally it increased to 77.3 kN at 75.6 mm. The energy absorption of the hybrid structure was 5.2 kJ, and 1.1 kJ higher than the energy absorption of SIC. Therefore, the force of this hybrid structure exhibited the characteristics of both the outer CFRP tube and the inner aluminum tube.

For C-PU-C, at the initial stage, the peak force of the hybrid structure was 26.2 kN less than SIC, mainly because the failure of the outer CFRP tube and the inner CFRP tube was not caused at the same time. During the compression process, the force of SIC changed little around 50.0 kN, and the force of the hybrid structure changed little around 70.0 kN, then it increased gradually when compression displacement reached about 70.0 mm, and it finally increased to 77.9 kN. The energy absorption of the hybrid structure was 5.4 kJ, which was 1.3 kJ higher than the energy absorption of SIC.

In general, the experimental results showed that the force and energy absorption of all hybrid structures increased compared with SIC. Firstly, the hybrid structures with application of CFRP tubes increased more than the pure aluminum structures. Secondly, the application of PU foam not only filled the space between the outer and inner tubes, it also changed their deformation mode, and then influenced the mechanical characteristics of the hybrid structures. During the compression process, the deformation of CFRP tubes was restricted by the PU foam filler; they extended outside or gathered inside with more friction and fiber breakage.

4.3. Simulation Results

Figures 9 and 10 show comparisons of the force–displacement curves and deformation modes of the simulation results and the experimental results for the single tubes and the hybrid structures, respectively. For the deformation mode, the simulation results matched the experimental results well; for example, there were concertina folds and diamond lobes in the single aluminum tube, and outward fronts and inward fronts in the single CFRP tube. In addition, the simulation solved the interaction between the individual components of the hybrid structures; the outer aluminum tubes were concertina folds, and the outer and inner CFRP tubes were outward fronts and inward fronts, respectively. For the force–displacement curves, the simulation results also matched the experimental results well. The force of the CFRP tubes fluctuated obviously; part of the reason for this was that the speed was much higher than the actual speed. A summary of the crashworthiness indicators for the single tubes and hybrid structures from the simulation results is presented in Table 4; the peak forces of the single tubes were lower than the experimental results,

while the other results showed good agreement with the experimental results. Figure 11 shows a comparison of the energy–displacement curves of internal energy (ALLIE), kinetic energy (ALLKE) and artificial strain energy (ALLAE) of AL-PU-AL and C-PU-C. ALLKE and ALLAE were much smaller than ALLIE, which means that the simulation met the quasi-static requirements. Summary of standard deviations of single tubes and hybrid structures obtained from the experiment and simulation results are in Table 5.

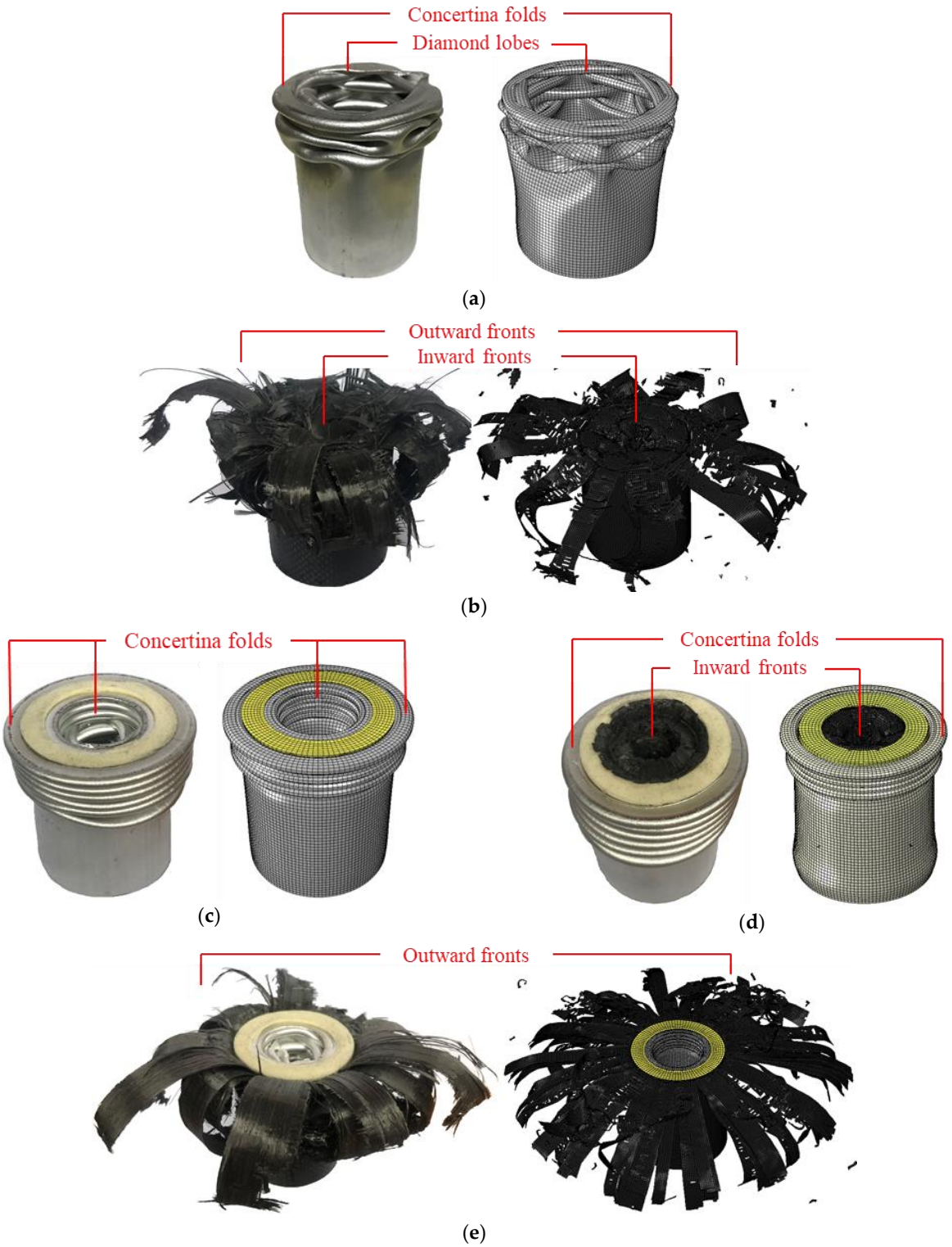

Figure 9. *Cont.*

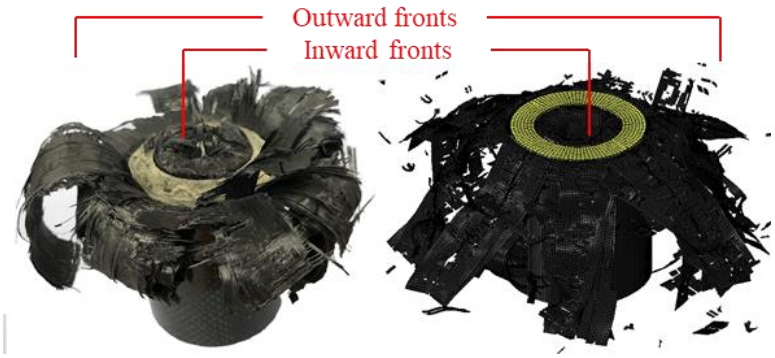

(**f**)

Figure 9. Comparison of deformation mode between the experimental results and simulation results: (**a**) AL-O; (**b**) C-O; (**c**) AL-PU-AL; (**d**) AL-PU-C; (**e**) C-PU-AL; (**f**) C-PU-C.

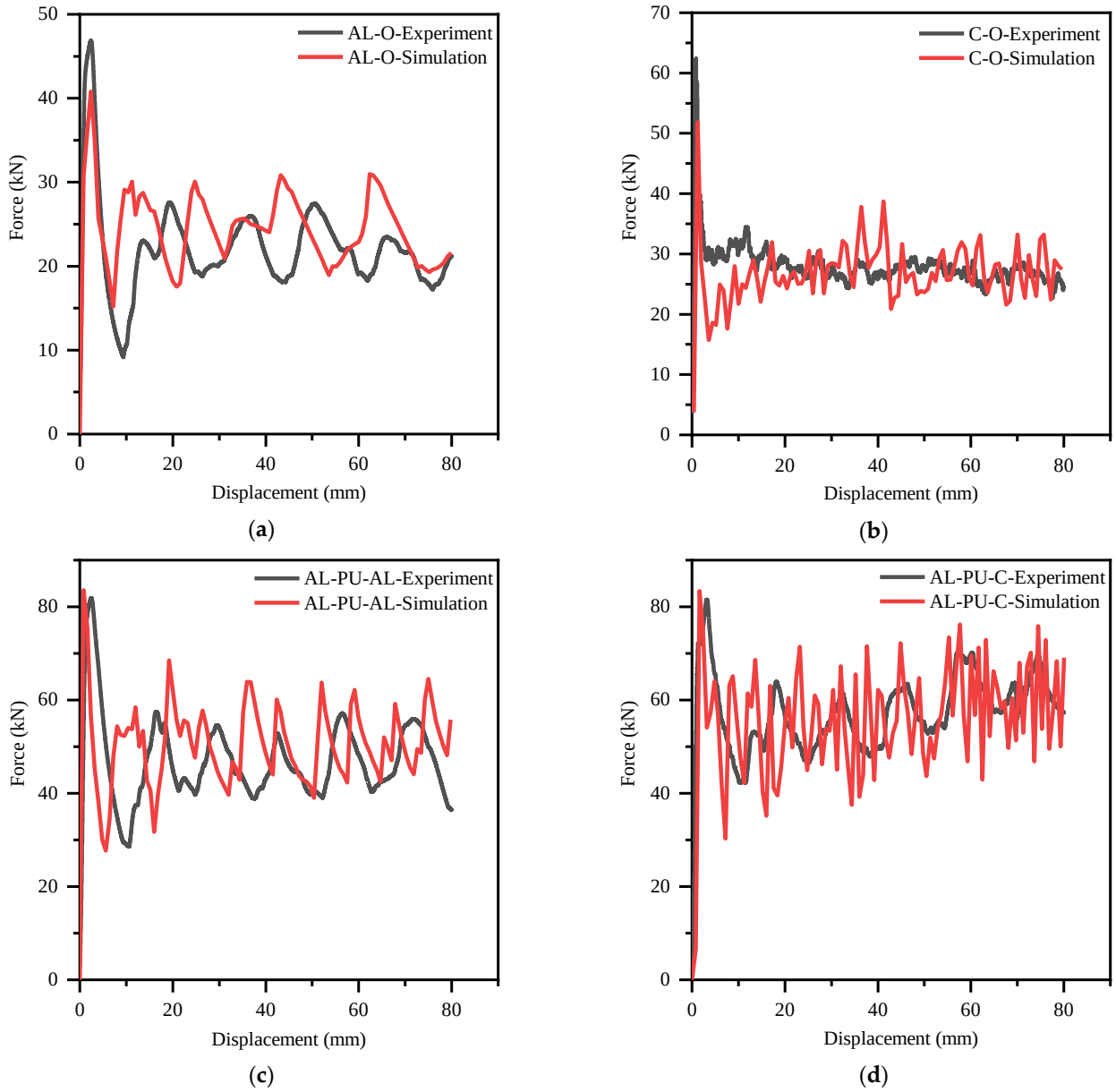

Figure 10. *Cont.*

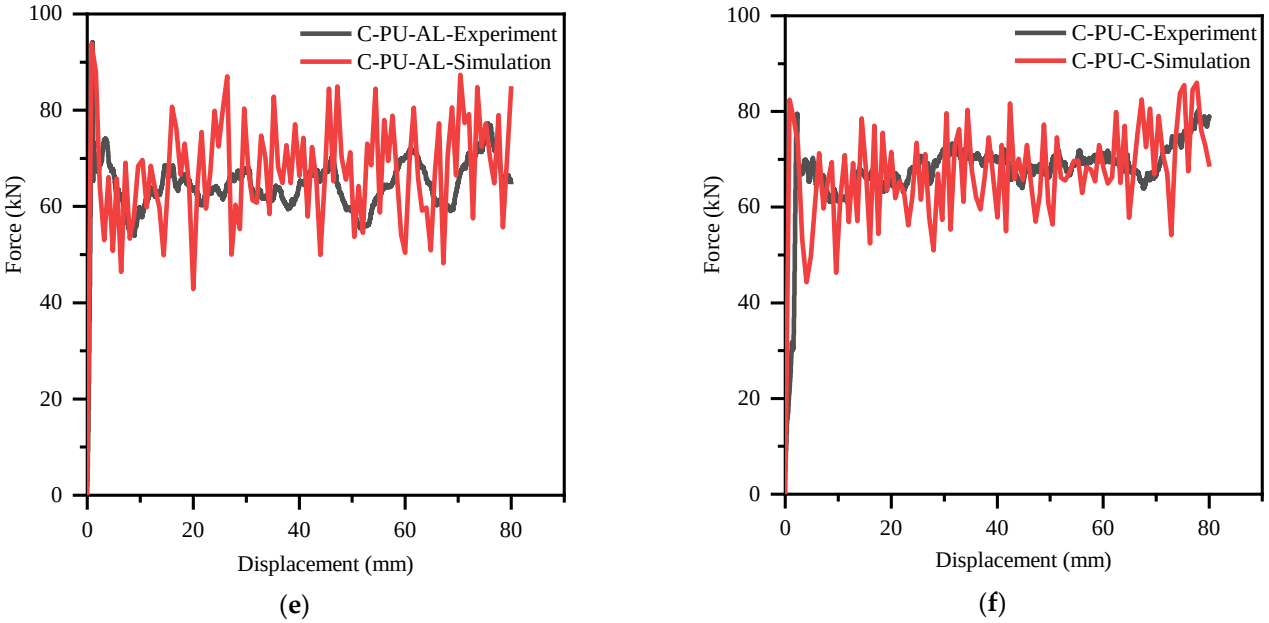

Figure 10. Comparison of force–displacement curves between the experimental results and simulation results: (**a**) AL-O; (**b**) C-O; (**c**) AL-PU-AL; (**d**) AL-PU-C; (**e**) C-PU-AL; (**f**) C-PU-C.

Table 4. Summary of crashworthiness indicators of single tubes and hybrid structures obtained from the simulation results.

Simulations	EA (kJ)	SEA (kJ/kg)	PF (kN)	MF (kN)
CFRP-O	2.2	34.1	51.7	27.5
AL-O	1.9	17.1	40.8	23.8
Foam-H	0.2	4.6	–	2.5
AL-PU-AL	4.0	18.3	83.5	50.0
AL-PU-C	4.5	23.5	83.4	56.3
C-PU-AL	5.3	30.9	93.8	66.3
C-PU-C	5.4	37.3	82.5	67.5

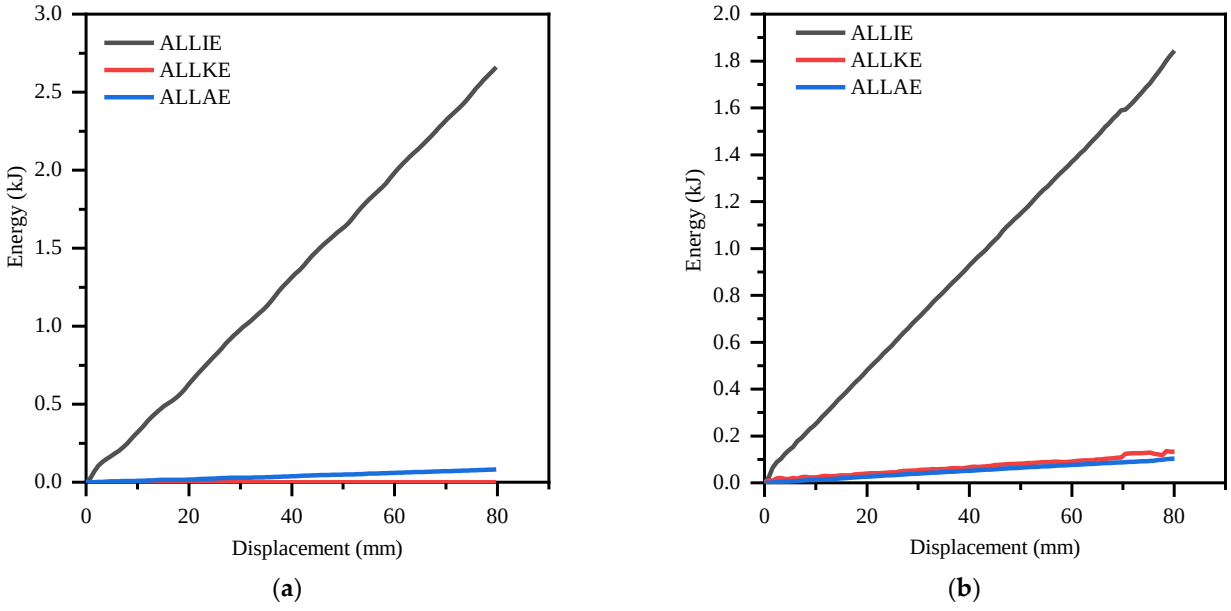

Figure 11. Comparison of energy–displacement curves between artificial strain energy (ALLAE), internal energy (ALLIE) and kinetic energy (ALLKE) of the simulation results: (**a**) AL-PU-AL; (**b**) C-PU-C.

Table 5. Summary of standard deviations of single tubes and hybrid structures obtained from the experiment and simulation results.

Specimen	EA	SEA	PF	MF
CFRP-O	0.3	0.7	3.2	2.2
AL-O	0.3	1.1	2.4	1.1
Foam-H	0.2	0.2	–	0.1
AL-PU-AL	0.5	1.2	1.3	1.9
AL-PU-C	0.3	0.7	1.4	1.1
C-PU-AL	0.3	0.8	0.5	1.2
C-PU-C	0.3	0.2	1.7	0.3

5. Conclusions

This study investigated the mechanical characteristics of four different polyurethane foam-filled hybrid structures and their individual components under quasi-static axial compression. The deformation mode and energy absorption of these experimental results were studied. Then, some economic indicators were considered in order to evaluate their energy absorption performance. Finally, numerical models were built and validated with respect to the experimental results. The following conclusions can be drawn:

1. Polyurethane foam-filled hybrid structures can change the deformation mode of individual tubes, and help to improve stability and energy absorption capacity during the compression process.
2. Polyurethane foam-filled hybrid structures can improve the energy absorption compared with their individual components. The energy absorption increases with the use of CFRP material, and the C-PU-C hybrid structure exhibited the highest energy absorption capacity, which is an obvious advantage in terms of lightweight design for energy absorption components.

Author Contributions: Conceptualization, S.Y. and Z.C.; methodology, Z.C.; software, Z.C.; validation, S.Y., Z.L. and Z.Z.; formal analysis, Z.C.; in-vestigation, Z.Z.; resources, S.Y.; data curation, Z.L.; writing—original draft preparation, Z.C.; writing—review and editing, Z.C.; visualization, Z.L.; supervision, P.X.; project administration, S.Y.; funding acquisition, P.X. All authors have read and agreed to the published version of the manuscript.

Funding: This research was funded by the National Key Research and Development Program of China, grant number 2016YFB1200505-016.

Institutional Review Board Statement: Not applicable.

Informed Consent Statement: Not applicable.

Data Availability Statement: The data that support the findings of this study are available from the corresponding author, upon reasonable request.

Conflicts of Interest: The authors declare no conflict of interest.

References

1. Li, S.; Guo, X.; Li, Q.; Ruan, D.; Sun, G. On lateral compression of circular aluminum, CFRP and GFRP tubes. *Compos. Struct.* **2020**, *232*, 111534. [CrossRef]
2. Zhang, W.; Qin, Q.; Li, J.; Li, K.; Poh, L.H.; Li, Y.; Zhang, J.; Xie, S.; Chen, H.; Zhao, J. Deformation and failure of hybrid composite sandwich beams with a metal foam core under quasi-static load and low-velocity impact. *Compos. Struct.* **2020**, *242*, 112175. [CrossRef]
3. Sebaey, T.A.; Mahdi, E. Filler strengthening of foam-filled energy absorption devices using CFRP beams. *Compos. Struct.* **2017**, *160*, 1–7. [CrossRef]
4. Sun, G.; Chen, D.; Wang, H.; Hazell, P.J.; Li, Q. High-velocity impact behaviour of aluminium honeycomb sandwich panels with different structural configurations. *Int. J. Impact Eng.* **2018**, *122*, 119–136. [CrossRef]
5. Bai, R.; Guo, J.; Lei, Z.; Liu, D.; Ma, Y.; Yan, C. Compression after impact behavior of composite foam-core sandwich panels. *Compos. Struct.* **2019**, *225*, 111181. [CrossRef]

6. Andrews, K.R.F.; England, G.L.; Ghani, E. Classification of the axial collapse of cylindrical tubes under quasi-static loading. *Int. J. Mech. Sci.* **1983**, *25*, 687–696. [CrossRef]
7. Yao, S.; Huo, Y.; Yan, K.; Xu, P. Crashworthiness study on circular hybrid corrugated tubes under axial impacts. *Thin-Walled Struct.* **2019**, *145*, 106358. [CrossRef]
8. Li, Z.; Ma, W.; Hou, L.; Xu, P.; Yao, S. Crashworthiness analysis of corrugations reinforced multi-cell square tubes. *Thin-Walled Struct.* **2020**, *150*, 106708. [CrossRef]
9. Ma, W.; Xie, S.; Li, Z. Mechanical performance of bio-inspired corrugated tubes with varying vertex configurations. *Int. J. Mech. Sci.* **2020**, *172*, 105399. [CrossRef]
10. Xu, P.; Xu, K.; Yao, S.; Yang, C.; Huang, Q.; Zhao, H.; Xing, J. Parameter study and multi-objective optimisation of an axisymmetric rectangular tube with diaphragms for subways. *Thin-Walled Struct.* **2019**, *136*, 186–199. [CrossRef]
11. Li, Z.; Yao, S.; Ma, W.; Xu, P.; Che, Q. Energy-absorption characteristics of a circumferentially corrugated square tube with a cosine profile. *Thin-Walled Struct.* **2019**, *135*, 385–399. [CrossRef]
12. Hussein, R.D.; Ruan, D.; Lu, G. An analytical model of square CFRP tubes subjected to axial compression. *Compos. Sci. Technol.* **2018**, *168*, 170–178. [CrossRef]
13. Zhu, G.; Sun, G.; Li, G.; Cheng, A.; Li, Q. Modeling for CFRP structures subjected to quasi-static crushing. *Compos. Struct.* **2018**, *184*, 41–55. [CrossRef]
14. Liu, Q.; Ma, J.; He, Z.; Hu, Z.; Hui, D. Energy absorption of bio-inspired multi-cell CFRP and aluminum square tubes. *Compos. Part B Eng.* **2017**, *121*, 134–144. [CrossRef]
15. Liu, Q.; Shen, H.; Wu, Y.; Xia, Z.; Fang, J.; Li, Q. Crash responses under multiple impacts and residual properties of CFRP and aluminum tubes. *Compos. Struct.* **2018**, *194*, 87–103. [CrossRef]
16. Zhu, G.; Liao, J.; Sun, G.; Li, Q. Comparative study on metal/CFRP hybrid structures under static and dynamic loading. *Int. J. Impact Eng.* **2020**, *141*, 103509. [CrossRef]
17. Wang, Z.; Jin, X.; Li, Q.; Sun, G. On crashworthiness design of hybrid metal-composite structures. *Int. J. Mech. Sci.* **2020**, *171*, 105380. [CrossRef]
18. Hussein, R.D.; Ruan, D.; Lu, G.; Thomson, R. An energy dissipating mechanism for crushing square aluminium/CFRP tubes. *Compos. Struct.* **2018**, *183*, 643–653. [CrossRef]
19. Huang, Z.; Zhang, X.; Yang, C. Static and dynamic axial crushing of Al/CRFP hybrid tubes with single-cell and multi-cell sections. *Compos. Struct.* **2019**, *226*, 111023. [CrossRef]
20. Yu, H.; Shi, H.; Chen, S. A novel multi-cell CFRP/AA6061 hybrid tube and its structural multiobjective optimization. *Compos. Struct.* **2019**, *209*, 579–589. [CrossRef]
21. Batuwitage, C.; Fawzia, S.; Thambiratnam, D.; Liu, X.; Al-Mahaidi, R.; Elchalakani, M. Impact behaviour of carbon fibre reinforced polymer (CFRP) strengthened square hollow steel tubes: A numerical simulation. *Thin-Walled Struct.* **2018**, *131*, 245–257. [CrossRef]
22. Jamil, A.; Guan, Z.W.; Cantwell, W.J. The static and dynamic response of CFRP tube reinforced polyurethane. *Compos. Struct.* **2017**, *161*, 85–92. [CrossRef]
23. Zhou, J.; Guan, Z.; Cantwell, W.J. The energy-absorbing behaviour of composite tube-reinforced foams. *Compos. Part B Eng.* **2018**, *139*, 227–237. [CrossRef]
24. Al Antali, A.; Umer, R.; Zhou, J.; Cantwell, W.J. The energy-absorbing properties of composite tube-reinforced aluminum honeycomb. *Compos. Struct.* **2017**, *176*, 630–639. [CrossRef]
25. Li, Z.; Chen, R.; Lu, F. Comparative analysis of crashworthiness of empty and foam-filled thin-walled tubes. *Thin-Walled Struct.* **2018**, *124*, 343–349. [CrossRef]
26. Sun, G.; Li, S.; Liu, Q.; Li, G.; Li, Q. Experimental study on crashworthiness of empty/aluminum foam/honeycomb-filled CFRP tubes. *Compos. Struct.* **2016**, *152*, 969–993. [CrossRef]
27. Zhu, G.; Wang, Z.; Huo, X.; Cheng, A.; Li, G.; Zhou, C. Experimental and numerical investigation into axial compressive behaviour of thin-walled structures filled with foams and composite skeleton. *Int. J. Mech. Sci.* **2017**, *122*, 104–119. [CrossRef]
28. Zheng, G.; Wang, Z.; Song, K. Energy absorption on metal-composite hybrid structures: Experimental and numerical simulation. *Thin-Walled Struct.* **2020**, *150*, 106571. [CrossRef]
29. Li, P.; Guo, Y.B.; Zhou, M.W.; Shim, V.P.W. Response of anisotropic polyurethane foam to compression at different loading angles and strain rates. *Int. J. Impact Eng.* **2019**, *127*, 154–168. [CrossRef]
30. Chen, J.; Fang, H.; Liu, W.; Zhu, L.; Zhuang, Y.; Wang, J.; Han, J. Energy absorption of foam-filled multi-cell composite panels under quasi-static compression. *Compos. Part B Eng.* **2018**, *153*, 295–305. [CrossRef]
31. Zhu, L.; Liu, W.; Fang, H.; Chen, J.; Zhuang, Y.; Han, J. Design and simulation of innovative foam-filled Lattice Composite Bumper System for bridge protection in ship collisions. *Compos. Part B Eng.* **2019**, *157*, 24–35. [CrossRef]
32. Wang, Y.; Lu, J.; Zhai, X.; Xue, B.; Zhi, X. Response of energy absorbing connector with polyurethane foam and multiple pleated plates under impact loading. *Int. J. Impact Eng.* **2019**, *133*, 103356. [CrossRef]
33. Wang, Y.; Pokharel, R.; Lu, J.; Zhai, X. Experimental, numerical, and analytical studies on polyurethane foam-filled energy absorption connectors under quasi-static loading. *Thin-Walled Struct.* **2019**, *144*, 106257. [CrossRef]
34. Li, Z.; Chen, W.; Hao, H. Functionally graded truncated square pyramid folded structures with foam filler under dynamic crushing. *Compos. Part B Eng.* **2019**, *177*, 107410. [CrossRef]

35. Li, Z.; Chen, W.; Hao, H. Dynamic crushing and energy absorption of foam filled multi-layer folded structures: Experimental and numerical study. *Int. J. Impact Eng.* **2019**, *133*, 103341. [CrossRef]
36. Hussein, R.D.; Ruan, D.; Lu, G.; Guillow, S.; Yoon, J.W. Crushing response of square aluminium tubes filled with polyurethane foam and aluminium honeycomb. *Thin-Walled Struct.* **2017**, *110*, 140–154. [CrossRef]
37. Gan, N.; Feng, Y.; Yin, H.; Wen, G.; Wang, D.; Huang, X. Quasi-static axial crushing experiment study of foam-filled CFRP and aluminum alloy thin-walled structures. *Compos. Struct.* **2016**, *157*, 303–319. [CrossRef]